Eur. Phys. J. D **25**, 239–246 (2003)
DOI: 10.1140/epjd/e2003-00206-6

THE EUROPEAN PHYSICAL JOURNAL D

Coupled-channel study with Coulomb wave packets for ionization of helium in heavy ion collisions*

I.F. Barna[a], N. Grün, and W. Scheid[b]

Institut für Theoretische Physik der Justus-Liebig-Universität, Heinrich-Buff-Ring 16, 35392 Giessen, Germany

Received 16 October 2002 / Received in final form 14 March 2003
Published online 15 July 2003

Abstract. The coupled-channel method is used to calculate excitation, single- and double-ionization cross-sections for helium collisions with heavy ions. The wave functions of the channels are helium wave functions constructed with Slater functions and Coulomb wave packets. Results of calculations with various projectiles and incident energies are compared with experimental data and other theoretical cross-sections.

PACS. 34.50.Fa Electronic excitation and ionization of atoms (including beam-foil excitation and ionization) – 34.10.+x General theories and models of atomic and molecular collisions and interactions (including statistical theories, transition state, stochastic and trajectory models, etc.)

1 Introduction

Ionization of the helium atom in collisions with fast highly charged ions is very interesting from both fundamental and applied points of view. The single-ionization for very fast, fully stripped ions colliding with light atoms is well understood both theoretically [1,2] and experimentally [3]. However for multiple ionization processes the level of knowledge is substantially lower. This is due to the fact that the electron-electron correlation plays an important role. Therefore, the theory should go beyond the independent-electron model. The role of the wave functions is essential as was shown by Byron and Joachain [4]. The experimental set-up for measurements has gained such a high quality and accuracy that the individual momenta of the two participating electrons and of the recoil ion become measurable (see [5,6]).

In this paper we study the two-electron problem of helium in collisions with highly charged ions within a coupled-channel formalism. As basis wave functions we take helium functions built up by Slater functions for the bound states and Coulomb wave packets for the continuum states. Such a basis was also used in stopping power and ionization calculations for the case of proton and light heavy ions penetrating into H and He targets [7]. This work is an extension of an earlier work of Pfeiffer *et al.* [8] where only Slater functions were used for the construction of helium states.

In Section 2 we present the theoretical basis of our calculations, namely the coupled-channel formalism, the helium wave functions for the individual channels and the separation of excitation, single- and double-ionization by a projection method. The results of coupled-channel calculations for various projectiles and incident energies are compared with experimental data and other theoretical studies in Section 3. Atomic units are used throughout the paper if not stated otherwise.

2 Theory

We describe the collision of a projectile ion with a helium atom as target in semiclassical approximation. The origin of the coordinates is the helium nucleus which is assumed to be fixed in the laboratory system. In this system we assume the projectile moving on a straight-line trajectory $\mathbf{R}_{\mathrm{P}}(t) = b\mathbf{e}_x + v_{\mathrm{P}}t\mathbf{e}_z$ with impact parameter b and constant velocity $\mathbf{v}_{\mathrm{P}} = v_{\mathrm{P}}\mathbf{e}_z$. The two electrons are described with the vectors $\mathbf{r}_1$ and $\mathbf{r}_2$.

The Hamiltonian of the system can be written

$$\hat{H} = \hat{H}_{\mathrm{He}} + \hat{V}, \tag{1}$$

where the Hamiltonian $\hat{H}_{\mathrm{He}}$ of the helium atom is assumed as

$$\hat{H}_{\mathrm{He}} = \frac{p_1^2}{2} + \frac{p_2^2}{2} - \frac{2}{r_1} - \frac{2}{r_2} + \frac{1}{|\mathbf{r}_1 - \mathbf{r}_2|}. \tag{2}$$

* This work is part of the doctoral thesis of I.F. Barna, Giessen (D26) 2002.

[a] *Present address*: Max-Planck-Institut für Physik komplexer Systeme, Dresden, Germany.
[b] e-mail: werner.scheid@physik.uni-giessen.de

The interaction with the projectile is given as

$$\hat{V} = \frac{1}{2}\left(\mathbf{A}(\mathbf{r}_1,t)\mathbf{p}_1 + \mathbf{p}_1\mathbf{A}(\mathbf{r}_1,t)\right) + \frac{1}{2}\left(\mathbf{A}(\mathbf{r}_2,t)\mathbf{p}_2 + \mathbf{p}_2\mathbf{A}(\mathbf{r}_2,t)\right) + \frac{1}{2}\left((\mathbf{A}(\mathbf{r}_1,t))^2 + (\mathbf{A}(\mathbf{r}_2,t))^2\right) - \varphi(\mathbf{r}_1,t) - \varphi(\mathbf{r}_2,t), \quad (3)$$

where $\mathbf{A}$ and φ are the electromagnetic potentials of the projectile in the target system.

2.1 Coupled-channel equations

In order to solve the time-dependent Schrödinger equation

$$\mathrm{i}\frac{\partial}{\partial t}\Psi(\mathbf{r}_1,\mathbf{r}_2,t) = \left(\hat{H}_{\mathrm{He}} + \hat{V}\right)\Psi(\mathbf{r}_1,\mathbf{r}_2,t), \quad (4)$$

we expand the wave function in orthonormalized eigenstates Φ_i of $\hat{H}_{\mathrm{He}}$ satisfying the eigenvalue equation with eigenvalues E_i

$$\hat{H}_{\mathrm{He}}\Phi_i(\mathbf{r}_1,\mathbf{r}_2) = E_i\Phi_i(\mathbf{r}_1,\mathbf{r}_2). \quad (5)$$

Then the wave function $\Psi(\mathbf{r}_1,\mathbf{r}_2,t)$ can be written with the time-dependent coefficients $a_i(t)$

$$\Psi(\mathbf{r}_1,\mathbf{r}_2,t) = \sum_{i=1}^{N} a_i(t)\Phi_i(\mathbf{r}_1,\mathbf{r}_2)\exp(-\mathrm{i}E_i t). \quad (6)$$

Inserting this relation into equation (4) we obtain

$$\frac{\mathrm{d}a_i(t)}{\mathrm{d}t} = -\mathrm{i}\sum_{j=1}^{N} V_{ij}(t)\exp(\mathrm{i}(E_i - E_j)t)a_j(t) \quad (7)$$

with

$$V_{ij}(t) = \left\langle \Phi_i|\hat{V}|\Phi_j \right\rangle. \quad (8)$$

Denoting the helium ground state with $i = 1$, we use the following initial conditions for solving equation (7):

$$a_i\left(t \to -\infty\right) = \begin{cases} 1 & \text{if} \quad i = 1, \\ 0 & \text{if} \quad i \neq 1. \end{cases} \quad (9)$$

Then the total cross-section for occupying the helium eigenstate i can be calculated as

$$\sigma_i = 2\pi\int_0^\infty P_i(b)b\mathrm{d}b \quad (10)$$

with the probability

$$P_i(b) = |a_i(t \to \infty)|^2. \quad (11)$$

The coupled system of equations (7) has to be solved numerically. However, approximate solutions for the coefficients $a_i(t)$ can be calculated in first-order perturbation theory for $i \neq 1$:

$$a_i(t) = -\mathrm{i}\int_{-\infty}^{t} V_{i1}(t')\exp(\mathrm{i}(E_i - E_1)t')\mathrm{d}t'. \quad (12)$$

The accuracy and range of validity of the first-order perturbation theory will be discussed in Section 3.

2.2 Approximate helium eigenstates

Since the helium is initially in the ground state and the Hamiltonian (1) does not mix singlet and triplet helium states, only singlet helium states enter the calculation. Therefore, we can disregard the spin part of the wave functions Φ_i and expand them in functions symmetric in the exchange of the coordinates $\mathbf{r}_1$ and $\mathbf{r}_2$

$$\Phi_{i=(\nu,LM)}(\mathbf{r}_1,\mathbf{r}_2) = \sum_{\mu} b_{\mu\nu}^{LM} f_{\mu}^{LM}(\mathbf{r}_1,\mathbf{r}_2) \quad (13)$$

with

$$f_{\mu}^{LM}(\mathbf{r}_1,\mathbf{r}_2) = \sum_{m_a,m_b} (\ell_a m_a \ell_b m_b|LM) \times \left(R_{n_a\ell_a}(r_1)R_{n_b\ell_b}(r_2)Y_{\ell_a m_a}(\vartheta_1,\varphi_1)Y_{\ell_b m_b}(\vartheta_2,\varphi_2) + R_{n_a\ell_a}(r_2)R_{n_b\ell_b}(r_1)Y_{\ell_a m_a}(\vartheta_2,\varphi_2)Y_{\ell_b m_b}(\vartheta_1,\varphi_1)\right) \quad (14)$$

and the abbreviation

$$\mu = (n_a, n_b, \ell_a, \ell_b).$$

For the radial single-particle wave functions $R_{n\ell}(r)$ we use hydrogen-like Slater functions mainly for the bound state spectrum and wave packets formed with regular Coulomb functions for the continua. The Slater functions read (no dependence on ℓ)

$$R_{n\ell}(r) = S_{\nu\kappa}(r) = c(\nu,\kappa)r^{\nu-1}\exp(-\kappa r) \quad (15)$$

with $n = (\nu,\kappa)$ and $c(\nu,\kappa) = (2\kappa)^{\nu+\frac{1}{2}}/\sqrt{(2\nu)!}$.

The functions $S_{\nu\kappa}$ are not orthogonal, but normalized to unity:

$$\int_0^\infty S_{\nu\kappa}^2(r)r^2\mathrm{d}r = 1. \quad (16)$$

The radial wave packets are constructed by an integral over regular Coulomb wave functions [9] in the interval $(E - \Delta E/2, E + \Delta E/2)$ corresponding to $(k - \Delta k/2 = (2E - \Delta E)^{1/2}, k + \Delta k/2 = (2E + \Delta E)^{1/2})$:

$$R_{n\ell}(r) = C_{k,\ell,\Delta k,Z}(r) = \frac{1}{\sqrt{\Delta E}}\int_{k-\frac{\Delta k}{2}}^{k+\frac{\Delta k}{2}} \sqrt{\frac{2k'}{\pi}}\exp\left(\frac{\pi Z}{2k'}\right)\frac{(2k'r)^\ell}{(2\ell+1)!}\exp(-\mathrm{i}k'r) \times |\Gamma(\ell+1-\mathrm{i}Z/k')|\,{}_1F_1(1+\ell+\mathrm{i}Z/k', 2\ell+2, 2\mathrm{i}k'r)k'\mathrm{d}k' \quad (17)$$

with $n = (k, \Delta k, Z)$. Here, Z is an effective charge number and is chosen $Z = 1$ for single-ionized basis states and $Z = 2$ for double-ionized basis states. The functions (17) are real and orthonormalized as follows

$$\int_0^\infty C_{k,\ell,\Delta k,Z}(r)C_{k',\ell,\Delta k,Z}(r)r^2\mathrm{d}r = \delta_{k,k'}. \quad (18)$$

The set of wave packets concentrated about the positive mean energies $E_n = (2n+1)\Delta E/2$ with $n = 0, 1, 2...$ simulates the single-particle states of the continuum.

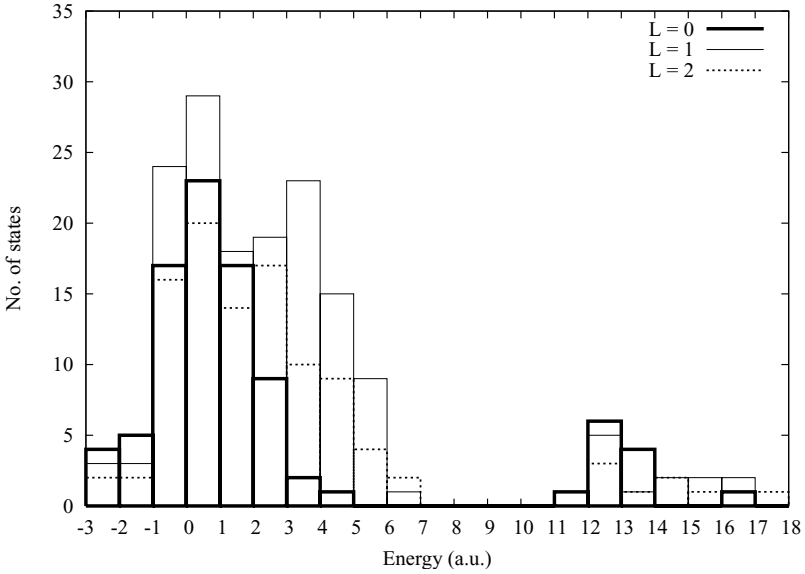

Fig. 1. Distribution of the diagonalized singlet states as a function of energy with $L = 0$, 1 and 2, presented as histograms with thick, thin and dotted lines, respectively.

Using an equidistant energy spacing of the wave packets, we managed to describe the low energy single- and double-continuum up to 6 a.u. We also tried to apply an equidistant spacing for the k values which yields a sparse state density with increasing energy and appears not so useful for our purpose.

Out of the single-particle states (15) and (17) we used 17 s-functions (9 Slater functions (sf), 4 wave packets (wp) with $Z = 1$ and 4 wp with $Z = 2$), 18 p-functions (6 sf, 6 wp with $Z = 1$ and 6 wp with $Z = 2$) and 12 d-functions (4 sf, 4 wp with $Z = 1$ and 4 wp with $Z = 2$) and constructed the symmetrized basis functions $f_\mu^{LM}(\mathbf{r}_1, \mathbf{r}_2)$. From the possible two-electron product states we selected 91 S-functions with configurations (s^2) and (s, s'), 156 P-functions with configurations (s, p) and 104 D-functions with configurations (s, d). The letters S, P, D stand for $L = 0, 1, 2$. We note that the M multiplicities, $M = 3$ and 5 for P and D states, respectively, are not contained in the above mentioned numbers of states. The effective charge in the wave packet is $Z = 1$ if the basis function $f_\mu^{LM}(\mathbf{r}_1, \mathbf{r}_2)$ contains a single wave packet and $Z = 2$ if the basis function is a product of two wave packets. Tables of the used single particle functions with their parameters are listed in reference [10].

As an example we give the chosen energy values of the 6 p Coulomb wave packets with $Z = 1$: 0.226, 0.417, 0.625, 0.828, 1.052, 1.238 a.u., and with $Z = 2$: 1.978, 2.470, 2.957, 3.436, 3.924, 4.432 a.u. The energy differences are about $\Delta E = 0.2$ and 0.5 a.u., respectively. The energies of the Coulomb wave packets with $Z = 2$ are taken higher than those with $Z = 1$ in order to describe double-ionized states also with one slower electron in an s-state and a faster electron in a p- and d-state.

Applying the three sets of basis functions $f_\mu^{LM}(\mathbf{r}_1, \mathbf{r}_2)$ with $L = 0, 1, 2$ and diagonalizing $\hat{H}_{\rm He}$, we obtained approximate wave functions $\Phi_{i=(\nu,LM)}(\mathbf{r}_1, \mathbf{r}_2)$ for the singlet states of He. The obtained energy eigenvalue of the ground state is -2.88 a.u. in comparison to the experimental value of -2.904 a.u. [11]. This deviation is due to the lack of angular correlated pp- and dd-functions. The diagonalization provides wave functions of the bound states and the states of the single and double continua with autoionizing bound states such as the $2s^2$-state embedded in the continuum. Figure 1 shows the distribution of the obtained He states as a function of the energy. The total numbers in the figure are 90 S-states (one state has an energy of 27.4 a.u. and is not included), 156 P-states and 104 D-states.

2.3 Separation of excitation, single- and double-ionization by a projection method

Since we want to calculate cross-sections for excitation, single- and double-ionization, we need the separate contributions of each state to these final reaction channels. In a former publication [8] we discriminated the states by examining the electron density. This method is not satisfactory in our case. Therefore, we constructed a new Hilbert space which is split into three different orthogonal subspaces characterized by the properties of the two electrons: 1 – bound-bound, 2 – bound-ionized, 3 – ionized-ionized electrons, respectively. The orthonormalized wave functions of these Hilbert spaces are obtained as follows: first, the same set of single-particle functions $R_{n\ell}(r)Y_{\ell m}(\vartheta, \varphi)$, used for the construction of the functions $f_\mu^{LM}(\mathbf{r}_1, \mathbf{r}_2)$, is taken and the Hamiltonian of hydrogen is diagonalized with it. Only wave packets with $Z = 1$ are used. The resulting single-particle functions $\tilde{R}_{s\ell}(r)Y_{\ell m}(\vartheta, \varphi)$ are orthonormalized and are bound, if the energy eigenvalue is smaller than zero, and in the continuum, if the energy eigenvalue is positive. Secondly, we construct with this set of single-particle functions the three subspaces of 2-electron functions:

$$\begin{aligned}\Psi_{\lambda,LM}(\mathbf{r}_1, \mathbf{r}_2) = (1/N_\lambda) \sum_{m_a,m_b} (\ell_a m_a \ell_b m_b | LM) \\ \times (\tilde{R}_{s_a\ell_a}(r_1)\tilde{R}_{s_b\ell_b}(r_2)Y_{\ell_a m_a}(\vartheta_1, \varphi_1)Y_{\ell_b m_b}(\vartheta_2, \varphi_2) \\ + \tilde{R}_{s_a\ell_a}(r_2)\tilde{R}_{s_b\ell_b}(r_1)Y_{\ell_a m_a}(\vartheta_2, \varphi_2)Y_{\ell_b m_b}(\vartheta_1, \varphi_1)) \quad (19)\end{aligned}$$

with $\lambda = (s_a, s_b, \ell_a, \ell_b)$ and $N_\lambda = \sqrt{2(1+\delta_{s_a s_b}\delta_{\ell_a \ell_b})}$.

If both radial functions $\tilde{R}_{s_a \ell_a}$ and $\tilde{R}_{s_b \ell_b}$ belong to negative eigenvalues, we classify $\Psi_{\lambda,LM} = \Psi^{\rm bb}_{\lambda,LM}$ as bound-bound function; if one of the radial functions belongs to a bound eigenvalue and the other radial function to the continuum, we classify $\Psi_{\lambda,LM} = \Psi^{\rm bi}_{\lambda,LM}$ as bound-ionized function; if both radial functions belong to the continuum, we classify $\Psi_{\lambda,LM} = \Psi^{\rm ii}_{\lambda,LM}$ as ionized-ionized function. Then we expand the He-functions (13) in terms of the functions (19):

$$\Phi_j(\mathbf{r}_1, \mathbf{r}_2) = \sum_\lambda \left(C^{\rm bb}_{\lambda j,LM} \Psi^{\rm bb}_{\lambda,LM} + C^{\rm bi}_{\lambda j,LM} \Psi^{\rm bi}_{\lambda,LM} + C^{\rm ii}_{\lambda j,LM} \Psi^{\rm ii}_{\lambda,LM} \right) \quad (20)$$

with

$$C_{\lambda j,LM} = \langle \Psi_{\lambda,LM} | \Phi_{j=(\nu,LM)} \rangle. \quad (21)$$

With the expansion coefficients $C_{\lambda j,LM}$ we find the portion of a bound (bb) configuration and of single (bi)- and double (ii)-ionized configurations in the wave function $\Phi_j(\mathbf{r}_1, \mathbf{r}_2)$:

$$\begin{aligned} A^{\rm bb}_j &= \sum_\lambda |C^{\rm bb}_{\lambda j,LM}|^2, \\ A^{\rm bi}_j &= \sum_\lambda |C^{\rm bi}_{\lambda j,LM}|^2, \\ A^{\rm ii}_j &= \sum_\lambda |C^{\rm ii}_{\lambda j,LM}|^2, \end{aligned} \quad (22)$$

where we assume completeness: $A^{\rm bb}_j + A^{\rm bi}_j + A^{\rm ii}_j = 1$.

Then the probabilities for the appearance of certain configurations after the collision are calculated as

$$\begin{aligned} P^{\rm bb}_j &= A^{\rm bb}_j |a_j(t \to \infty)|^2, \\ P^{\rm bi}_j &= A^{\rm bi}_j |a_j(t \to \infty)|^2, \\ P^{\rm ii}_j &= A^{\rm ii}_j |a_j(t \to \infty)|^2. \end{aligned} \quad (23)$$

These probabilities are used for calculating the cross-sections for the excitation of helium, the single- and double-ionization by inserting them into equation (10) and summing over j if needed.

2.4 The projectile-electron interaction

The electromagnetic potentials of the projectile are assumed in the form of Lienard-Wiechert potentials

$$\varphi(\mathbf{r}, t) = \frac{\gamma_{\rm P} Z_{\rm P}}{R(t)}, \qquad \mathbf{A}(\mathbf{r}, t) = \frac{1}{c^2} \frac{\gamma_{\rm P} v_{\rm P} Z_{\rm P}}{R(t)} \mathbf{e}_z \quad (24)$$

with

$$\gamma_{\rm P} = (1 - v_{\rm P}^2/c^2)^{-1/2}$$
$$\text{and} \quad R(t) = ((x-b)^2 + y^2 + \gamma_{\rm P}^2 (z - v_{\rm P} t)^2)^{1/2}.$$

Table 1. State-selective excitation cross-sections for 1 MeV proton projectiles. The units are 10^{-18} cm^2.

	Experimental data [12]	Coupled-channel calculations
$\sigma(2^1{\rm P})$	4.91	4.72
$\sigma(3^1{\rm P})$	1.26	1.31
$\sigma(4^1{\rm P})$	0.53	0.54

Inserting these potentials into equation (3) we obtain the projectile-electron interaction

$$\begin{aligned} \hat{V} = &- {\rm i} v_{\rm P} \gamma_{\rm P} Z_{\rm P} \frac{1}{c^2} \left(\frac{1}{R_1(t)} \frac{\partial}{\partial z_1} + \frac{1}{R_2(t)} \frac{\partial}{\partial z_2} \right) \\ &- \gamma_{\rm P} Z_{\rm P} \left(\frac{1}{R_1(t)} + \frac{1}{R_2(t)} \right) \\ &+ \frac{v_{\rm P}^2 \gamma_{\rm P}^2 Z_{\rm P}^2}{2c^4} \left(\frac{1}{R_1(t)^2} + \frac{1}{R_2(t)^2} \right) \\ &+ {\rm i} \frac{v_{\rm P} \gamma_{\rm P}^3 Z_{\rm P}}{2c^2} \left(\frac{z_1 - v_{\rm P} t}{R_1(t)^3} + \frac{z_2 - v_{\rm P} t}{R_2(t)^3} \right), \end{aligned} \quad (25)$$

where $R_i(t) = ((x_i - b)^2 + y_i^2 + \gamma_{\rm P}^2 (z_i - v_{\rm P} t)^2)^{1/2}$ with $i = 1, 2$.

The results of Pfeiffer *et al.* [8] showed that it is satisfactory to use only the scalar potential terms for incident energies with $\gamma_{\rm P} < 3.2$, corresponding to 2 GeV/nucleon. Therefore, we neglect the terms containing the vector potential $\mathbf{A}$ and set the projectile-electron interaction equal to the unretarded scalar potential

$$\hat{V} = -Z_{\rm P} \left(\frac{1}{R_1(t)} + \frac{1}{R_2(t)} \right)_{\gamma_{\rm P}=1}. \quad (26)$$

The method of the calculation of the matrix elements of $\hat{V}$ with the Slater functions and wave packets is described in [10].

3 Results

The coupled-channel equations were numerically solved by using a Runge-Kutta-Fehlberg method of fifth order with time steps automatically regulated. The conservation of the norm of the wave function was fulfilled better than 10^{-8} during the collision time. We chose projectile energies and charges for cases where the electron capture process can be neglected.

3.1 Calculations of excitation cross-sections

The first calculations were test calculations to reproduce the measured cross-sections for state-selective excitation of helium in collisions with 1 MeV protons. The comparison of results from our coupled-channel calculations with experimental data of Hippler and Schartner [12] is given in Table 1. Our results are affected by 1–2% by the usage of wave packets in the basis, as calculations with and without wave packets have demonstrated.

Table 2. Single- and double-ionization cross-sections for 3.6 MeV proton projectiles.

	Single-ion. $\sigma^+(10^{-19}$ cm$^2)$	Double-ion. $\sigma^{++}(10^{-21}$ cm$^2)$	Ratio $(\times 10^{-3})$
Exp. [13]	70.7	19.2	2.71
CC calc. [8]	58.58	6.59	1.12
Present CC calc.	66.52	18.66	2.80
FIM [15] $9s9p5d$	68.2	23.69	3.03
FIM [15] $9s9p9d$	70.0	18.9	2.70

Table 3. Single- and double-ionization cross-sections for 3.6 MeV anti-proton projectiles.

	Single-ion. $\sigma^+(10^{-19}$ cm$^2)$	Double-ion. $\sigma^{++}(10^{-21}$ cm$^2)$	Ratio $(\times 10^{-3})$
Exp. [14]	70.08	27.9	3.98
Present CC calc.	66.11	25.12	3.8
FIM [15] $9s9p5d$	68.2	28.6	4.2
FIM [15] $9s9p9d$	70.04	27.7	3.96

Table 4. Single-ionization total cross-sections obtained with coupled-channel calculations and with first-order perturbation approximation.

Proj.	Energy MeV/nucl.	Z_P/v_P a.u.	Exp. value $(10^{-16}$ cm$^2)$	CC calc. $(10^{-16}$ cm$^2)$	Pert. calc. $(10^{-16}$ cm$^2)$
U^{92+}	1000	0.76	$7.4 \pm 30\%$	4.8	
U^{90+}	60	1.92	13 –77% +150%	12.1	
U^{90+}	120	1.41	38 –50% +190%	9.7	
U^{90+}	420	0.91	9.8 –70% +200%	8.1	
Kr^{36+}	500	0.36	$0.9 \pm 50\%$	1.09	3.2
Kr^{36+}	1000	0.30	$0.72 \pm 50\%$	0.9	2.9
C^{6+}	100	0.1	0.1	0.097	0.11
He^{2+}	2.31	0.20	$0.44 \pm < 5\%$	0.40	0.46
Li^{3+}	”	0.31	$0.98 \pm < 5\%$	0.90	1.038
B^{5+}	”	0.51	$2.44 \pm < 8\%$	2.11	2.88
C^{6+}	”	0.62	$3.3 \pm < 8\%$	3.05	4.15

3.2 Single- and double-ionization with proton and anti-proton projectiles

We made coupled-channel calculations for proton and anti-proton collisions with helium at 3.6 MeV. In atomic units the projectile velocity is $v_P = 12$ a.u. and the ratio $Z_P/v_P = 0.08$ which means that perturbative calculations are also possible. Tables 2 and 3 present our results for proton and anti-proton collisions, respectively, in comparison with experimental data [13,14], coupled-channel calculations of Pfeiffer *et al.* [8] and with results of Ford and Reading [15] obtained with the Forced Impulse Method (FIM) which are considered as benchmark. Pfeiffer *et al.* [8] took only Slater functions and no wave packets into account. The comparison of both coupled-channel calculations in Table 2 shows that the wave packets are important to reproduce the double-ionization cross-section, *i.e.* the continua are better described with wave packets than with Slater functions only.

The FIM results are still better than our results. One reason is that Ford and Reading [15] used larger sets of He basis states, namely 1093 states for the $9s9p5d$ basis and 1863 states for the $9s9p9d$ basis, which has to be compared to 277 channels applied in our calculations.

3.3 Heavy ion projectiles

Next we chose the following projectiles and energies in collisions with helium which were experimentally studied:

1. U^{92+} at 1 GeV/nucleon (Moshammer *et al.* [6]),
2. U^{90+} at 60, 120, 420 MeV/nucleon (Berg *et al.* [16]),
3. Kr^{36+} at 500 and 1000 MeV/nucleon (Berg *et al.* [17]),
4. C^{6+} at 100 MeV/nucleon (Bapat *et al.* [18]),
5. He^{2+}, Li^{3+}, B^{5+}, C^{6+} at 2.31 MeV/nucleon (Knudsen *et al.* [19]).

Tables 4 and 5 show the single- and double-ionization total cross-sections, respectively, measured in experiment and calculated with the coupled-channel method and with

Table 5. Double-ionization total cross-sections obtained with coupled-channel calculations and with first-order perturbation approximation.

Proj.	Energy MeV/nucl.	Z_P/v_P a.u.	Exp. value (10^{-16} cm^2)	CC calc. (10^{-16} cm^2)	Pert. calc. (10^{-16} cm^2)
U^{92+}	1000	0.76	0.15 ± 30%	0.14	
U^{90+}	60	1.92	0.9 –70% +200%	0.81	
U^{90+}	120	1.41	1.8 –50% +100%	0.54	
U^{90+}	420	0.91	0.28 –70% +200%	0.38	
Kr^{36+}	500	0.36	0.016 ± 50%	0.010	0.07
Kr^{36+}	1000	0.30	0.011 ± 50%	0.012	0.016
C^{6+}	100	0.1	0.00026	0.00022	0.0003
He^{2+}	2.31	0.20	0.0022 ± < 10%	0.0026	0.003
Li^{3+}	”	0.31	0.0085 ± < 10%	0.0059	0.007
B^{5+}	”	0.51	0.059 ± < 11%	0.032	0.015
C^{6+}	”	0.62	0.092 ± < 11%	0.15	0.025

Table 6. The ratio $R = \sigma^{++}/\sigma^{+}$ obtained with the cross-sections of Tables 4 and 5.

Proj.	Energy MeV/nucl.	γ_P	v_P a.u.	Z_P/v_P a.u.	Exp. value ($\times 10^{-3}$)	CC calc. ($\times 10^{-3}$)	Pert. calc. ($\times 10^{-3}$)
U^{92+}	1000	2.07	120.01	0.76	20.27 ± 30%	29.1	
U^{90+}	60	1.06	46.58	1.92	63 –40% +33%	67	
U^{90+}	120	1.12	63.43	1.41	50 –35% +25%	55	
U^{90+}	420	1.45	98.64	0.91	30 –40% +33%	47	
Kr^{36+}	500	1.53	98.71	0.36	17.2	9.1	10.7
Kr^{36+}	1000	2.07	120.01	0.30	14.3	13	2.7
C^{6+}	100	1.1	58.76	0.1	2.6	2.6	2.72
He^{2+}	2.31	1.002	9.65	0.20	5.0 ± < 9%	6.5	6.5
Li^{3+}	”	”	”	0.31	8.6 ± < 9%	6.5	6.7
B^{5+}	”	”	”	0.51	24.3 ± < 9%	15.1	5.2
C^{6+}	”	”	”	0.62	28.0 ± < 9%	49.1	6.32

the first-order perturbative expression (12). The ratios between the single- and double-ionization total cross-sections are listed in Table 6. If the parameter Z_P/v_P, given in Tables 4–6, is larger than 0.5, the perturbation calculation is no more valid.

In the coupled-channel calculations given in Tables 2–6 always 277 channels were used. This number was the maximum which we could treat on our work stations. However, different sets of coupled channels were chosen for describing the continua, depending on the Lorentz factor and the charge of the projectile. In the case of fast collisions with the projectiles U^{92+}, U^{90+}, Kr^{36+} and C^{6+} (100 MeV/nucleon), channels up to a maximum energy of 28 a.u. were applied. In the other cases with the projectiles He^{2+}, Li^{3+}, B^{5+}, and C^{6+} (2.31 MeV/nucleon) only channels up to an energy of 6 a.u. were selected. The spectrum of occupation probabilities as a function of energy shows that mainly the channels with energies up to 5 a.u. and with angular momentum $L = 1$ get occupied.

The $\mathbf{A}^2$-term in expression (25) scales with $\gamma_P^2 Z_P^2$. In the case of the U^{92+}(1 GeV/nucleon)-projectile, this term is of the order of the scalar potential term. Therefore, we included the $\mathbf{A}^2$-term for this collision system in our calculations and obtained the single-ionization cross-section as 7.2 $\times 10^{-16}$ cm^2 instead of 4.8 $\times 10^{-16}$ cm^2 in Table 4 and the double-ionization cross-section as 0.16 $\times 10^{-16}$ cm^2 instead of 0.14 $\times 10^{-16}$ cm^2 in Table 5. The ratio is 0.022 instead of 0.029 in Table 6.

In Figures 2 and 3 we show scaled experimental and theoretical single- and double-ionization cross-sections, respectively. The comparison of the calculations with experimental data is difficult to interpret. As indicated in Tables 4–6 the experimental data have certain error bars which are quite large for higher incident energies. For example, the cross-sections for single- and double-ionization of He with U^{90+} projectiles should go steadily down with increasing incident energy which is not the case in the given experimental values. On the theoretical side, we can presently not claim that the used set of basis functions is already sufficiently complete for the considered cases. The number of channels increases fast with a finer distribution of the mean energies of the continuum states and is practically limited by the available computer time.

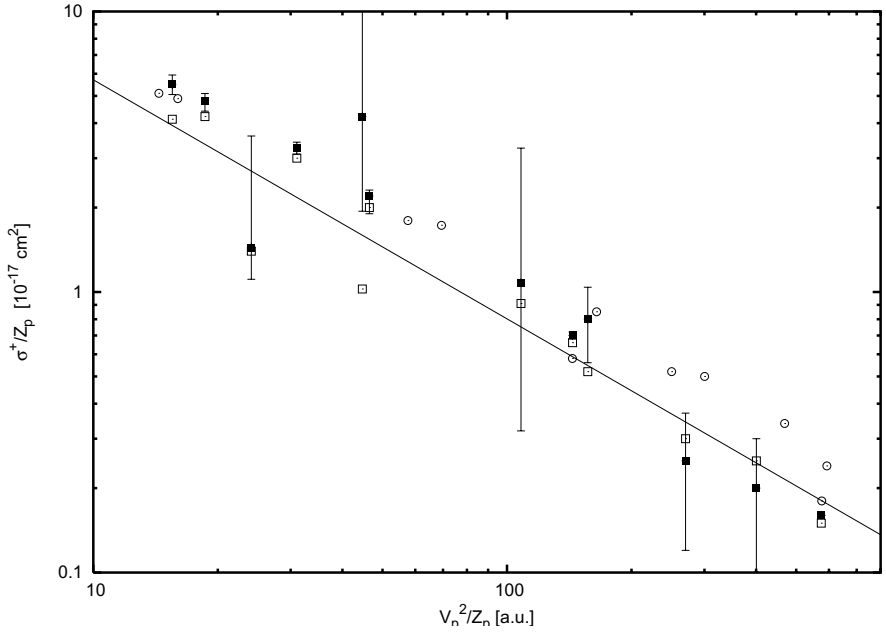

Fig. 2. Scaled single-ionization cross-section σ^+/Z_P of Tables 2 and 4 as a function of $v_\mathrm{P}^2/Z_\mathrm{P}$ presented on a double-logarithmic scale. The full squares are the experimental data (see [6,13,16–19]). The open squares are the present coupled-channel results. The full line is a regression line through our data points according to equation (27). The open circles are coupled-channel results of Pfeiffer *et al.* [8].

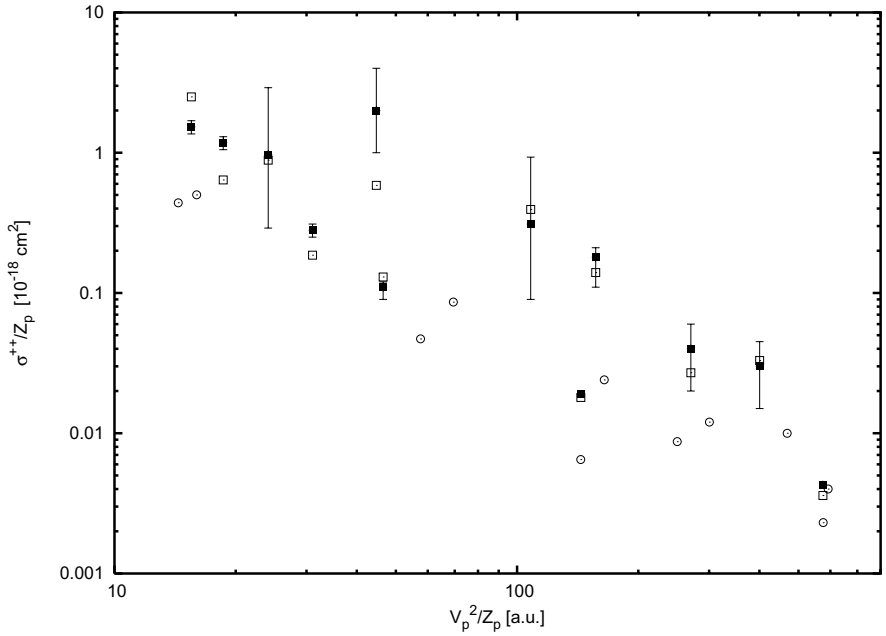

Fig. 3. Scaled double-ionization cross-section σ^{++}/Z_P of Tables 2 and 5 as a function of $v_\mathrm{P}^2/Z_\mathrm{P}$ presented on a double-logarithmic scale. The full squares are the experimental data (see [6,13,16–19]). The open squares are the present coupled-channel results. The open circles are coupled-channel results of Pfeiffer *et al.* [8].

The single-ionization cross-section can be presented by a scaling law which is the straight line through our calculated results in the double-logarithmic Figure 2. This line is given by

$$\frac{\sigma^+}{Z_\mathrm{P}} = 10^{0.60}\left(\frac{v_\mathrm{P}^2}{Z_\mathrm{P}}\right)^{-0.84} \times 10^{-16} \quad \mathrm{cm}^2. \qquad (27)$$

Such a scaling law with the use of σ^+/Z_P *versus* $v_\mathrm{P}^2/Z_\mathrm{P}$ was first introduced by Olson *et al.* [20]. The double-ionization cross-section can not be described by a similar scaling law.

There was some debate about the importance of static and dynamic correlations in double ionization of He. According to the textbook of McGuire [21] one speaks of static correlations if the emphasis lays on evaluating energy levels, while dynamic correlations play a role for transition probabilities and cross-sections. In our calculations the basis wave functions contain the static correlations due to the electron-electron interaction. The amplitudes of the He basis wave functions get mixed by the time-dependent one-particle potential of the projectile. This description of the reaction process does not allow to interpret the ionization process in terms of dynamical correlations, *i.e.*, whether an ionized electron induces the ionization of the second electron *via* the electron-electron repulsion. However, such processes are hidden in our basis expansion.

4 Summary and conclusions

We have presented coupled-channel and first order perturbation calculations of cross-sections for single- and double-ionization of helium in heavy ion collisions. As projectile-electron interaction we used the unretarded scalar potential of the projectile. The set of the channels were helium wave functions built up by Slater functions mainly for the bound states and Coulomb wave packets for the continua. A method for discriminating excitation, single and double ionization of the electrons was developed by applying a projection with an orthonormalized basis set of two-electron wave functions.

The convergence properties of the coupled-channel model were discussed for the proton-helium collision. In this case the advantage of wave packets in contrast of using only Slater functions was demonstrated. We investigated collisions of U^{92+}, U^{90+}, Kr^{36+}, He^{2+}, Li^{3+}, B^{5+} and C^{6+} projectiles with helium and found a good agreement of single- and double-ionization total cross-sections with experimental data in general.

Further calculations have to be carried out for cross-sections differential in the emission angles and energies of the electrons, where experimental data are available for comparison with theory. Also the projection formalism for distinguishing the excitation and ionization needs further developments.

References

1. M. Inokuti, Rev. Mod. Phys. **42**, 297 (1971)
2. M. Inokuti, Rev. Mod. Phys. **50**, 23 (1978)
3. H.K. Haugen, L.H. Andersen, P. Hvelplund, H. Knudsen, Phys. Rev. A **26**, 1950 (1982)
4. F. Byron, C.J. Joachain, Phys. Rev. Lett. **16**, 1139 (1966)
5. J. Ullrich, R. Moshammer, R. Dörner, O. Jagutzki, V. Mergel, H. Schmidt-Böcking, L. Spielberger, J. Phys. B: At. Mol. Opt. Phys. **30**, 2917 (1997)
6. R. Moshammer, W. Schmitt, J. Ullrich, H. Kollmus, A. Cassimi, R. Dörner, O. Jagutzki, R. Mann, R.E. Olson, H.T. Prinz, H. Schmidt-Böcking, L. Spielberger, Phys. Rev. Lett. **79**, 3621 (1997)
7. P.L. Grande, G. Schiwietz, Phys. Rev. A **47**, 1119 (1992)
8. C. Pfeiffer, N. Grün, W. Scheid, J. Phys. B: At. Mol. Opt. Phys. **32**, 53 (1999)
9. M. Abramowitz, A. Stegun, *Handbook of Mathematical Functions* (Dover Publications Inc., New York, 1972)
10. I. Barna, doctoral thesis, University Giessen, unpublished, 2002
11. C.E. Moore, *Atomic Energy Levels*, Nat. Stand. Ref. Data Ser., NBS (Washington D.C., 1971), No. 35, Vols. I–III
12. R. Hippler, K.-H. Schartner, J. Phys. B: At. Mol. Opt. Phys. **7**, 618 (1974)
13. M.B. Shah, H.B. Gilbody, J. Phys. B: At. Mol. Opt. Phys. **18**, 899 (1985)
14. P. Hvelplund, H. Knudsen, U. Mikkelsen, E. Morenzoni, S.P. Moller, E. Uggerhoj, T. Worm, J. Phys. B: At. Mol. Opt. Phys. **27**, 925 (1994)
15. A.L. Ford, J.F. Reading, J. Phys. B: At. Mol. Opt. Phys. **27**, 4215 (1994)
16. H.E. Berg, O. Jagutzki, R. Dörner, R.D. Dubois, C. Kelbach, H. Schmidt-Böcking, J. Ullrich, J.A. Tanis, A. Schlachter, L. Blumenfeld, B. d'Etat, S. Hagmann, A. Gonzales, T. Quinteros, Phys. Rev. A **46**, 5539 (1992)
17. H.E. Berg, J. Ullrich, E. Bernstein, M. Unverzagt, L. Spielberger, J. Euler, D. Schardt, O. Jagutzki, H. Schmidt-Böcking, R. Mann, P.H. Mokler, S. Hagmann, P.D. Fainstein, J. Phys. B: At. Mol. Opt. Phys. **25**, 3655 (1992)
18. B. Bapat, R. Moshammer, S. Keller, W. Schmitt, A. Cassimi, L. Adoui, H. Kollmus, R. Dörner, Th. Weber, K. Khayyat, R. Mann, J.P. Grandin, J. Ullrich, J. Phys. B: At. Mol. Opt. Phys. **32**, 1859 (1998)
19. H. Knudsen, L.A. Andersen, P. Hvelplund, C. Astner, H. Cederquist, H. Danared, L. Liljeby, K.-G. Rensfelt, J. Phys. B: At. Mol. Opt. Phys. **17**, 3545 (1984)
20. R.E. Olson, K.H. Berkner, W.G. Graham, R.V. Pyle, A.S. Schlachter, J.W. Stearns, Phys. Rev. Lett. **41**, 163 (1978)
21. J.H. McGuire, *Electron Correlation Dynamics in Atomic Collisions* (Cambridge University Press, 1977), p. 124